Monitoring Precipitable Water Vapor in Real-Time using Kinematic GPS Precise Point Positioning in Thailand

Charoenphon, C.[1] and Satirapod, C.[2*]
Department of Survey Engineering, Chulalongkorn University, Bangkok, Thailand
E-mail: chaiyut.c@student.chula.ac.th,[1] chalermchon.s@chula.ac.th[2]
**Corresponding author*

Abstract
The Global Navigation Satellite System (GNSS) in meteorology known as GNSS-Meteorology is an alternative way to estimate the PWV values, which is fewer data processing load and cost-effective. In the last two decades, several studies have shown that the estimated PWV values derived from ground-based GNSS receivers are nearly proportional to the amount of PWV from the meteorological instruments. Moreover, it has the advantages in high spatio-temporal resolution. In this study, Precise Point Positioning (PPP) technique was used to process the GNSS observation data. The CLK91 real-time orbit and clock products generated to the broadcast ephemeris based on the International GNSS Service (IGS) network were adopted in the data processing step. In order to accurately transform the zenith tropospheric delay (ZTD) into the PWV, the meteorological data and the local mean tropospheric temperature model (Tm) were evaluated for this study. The results showed that the different ZTD values of most stations, about 80% of the real-time epoch solution, were within 20 mm.

1. Introduction

The application of the Global Navigation Satellite System (GNSS) in meteorology known as GNSS-Meteorology has been intensively studied more than three decades. Ground-based GNSS receivers could provide the estimated tropospheric Zenith Total Delay (ZTD) or Precipitable Water Vapor (PWV) values with an accuracy comparable to the meteorological instruments such as radiosondes and microwave radiometers (Hagemann et al., 2003 and Li et al., 2015). Compared to the conventional meteorological instruments, GNSS-Meteorology shows various advantages, for instance, fewer data processing load, cost-effective, all-weather availability, and high spatio-temporal resolution. Various tests have been conducted to evaluate GPS-PWV in post-processing and near-real-time technique. An assessment on GPS-PWV using International Global Navigation Satellite Systems Service (IGS) ultra-rapid orbit data were conducted by Satirapod et al., (2011). The results addressed the potential use of ultra-rapid orbits for a near-real-time estimation of PWV. Near-real-time GPS-PWV was applied in numerical weather prediction and showed 2% improvement for the relative humidity in a 12-hour forecast (Gendt et al., 2004). Assimilation of GPS-ZTD observations has been shown to give some improvements in the forecasting of cloud (Bennitt and Jupp, 2012).

In order to estimate GNSS ZTD/PWV, there are two data processing techniques: the baseline/network approach (Elgered et al., 1991) and Precise Point Positioning (PPP) approach (Zumberge et al., 1997). The baseline/network approach is complex in terms of selection of baseline and the data processing load when the number of stations has increased. The PPP approach is based on Un-Differenced (UD) observations and displays its unique advantages to applications compared to the baseline/network (Yuan et al., 2014). In the PPP approach, the base station is not required; thus, data processing time is relative to the number of stations and ZTD/PWV values can be estimated epoch by epoch, which is really useful for the meteorological applications that require near-real-time or real-time ZTD/PWV values (Grinter and Roberts, 2013). Kitpracha et al., (2017) investigated the precise tropospheric delay using the GNSS PPP technique with the Positioning and Navigation Data Analyst (PANDA) software. Results obtained from the PPP technique showed a good agreement with the IGS product at the millimeter level. Meunram and Satirapod (2018) studied the variation of PWV using PPP technique to determine the coverage distance from GNSS station in Thailand. This study confirmed that GNSS observations could be applied to meteorological application.

Since April 2013, the precise real-time satellite orbit and clock products have been released from the IGS Real-Time Pilot Project (IGS-RTPP) through Networked Transport of RTCM (Radio Technical Commission of Maritime Services) via Internet Protocol (NTRIP) (Weber et al., 2016). Product quality and essential explanations of these products are available at the official Real-Time Service (RTS) webpage. These products are highly useful opportunities and challenges for real-time PPP of ZTD/PWV values for atmospheric and disaster monitoring, especially for now casting.

Several studies of the real-time PPP technique using GPS or GNSS data from Continuously Operating Reference Station (CORS) networks have been investigated and proven that GNSS-derived ZTD/PWV values can be shown a positive impact on NWP and applied for weather forecasting (Dousa and Vaclavovic, 2014 and Rohm et al., 2014). Over the last 2-3 years, GNSS techniques have rapidly developed. In terms of the increasing number of satellites, GNSS CORS networks, and correction products that are used to estimate the position quickly, accurately. Those developments are vastly useful for estimated ZTD/PWV values, especially for time-critical meteorological applications (Lu et al., 2015 and Shi et al., 2015). In Thailand, GNSS Real-Time-Kinematic (RTK) network infrastructure project was established in 2016 and will be completed in 2018 with about 222 CORS stations to support surveying, precise positioning, land governance, and cadastral operations. There is a good opportunity to evaluate ZTD/PWV values in Thai-land. Also, the variation of estimated ZTD values in this region is more challenging than other places (Li et al., 2012 and Yuan et al., 2014). In this preliminary study, the Federal Agency for Cartography and Geodesy (BKG) NTRIP Client (BNC) version 2.12.3 software platform (Weber et al., 2016), which uses the Ionosphere-free combinations together with Extended Kalman Filter (EKF) techniques to estimate the receiver position, the receiver clock bias and ZTD, was used to process the GPS data. Although GNSS observations were available, only GPS observations were processed. The CLK91 products generated from CNES to the broadcast ephemeris were adopted in the data processing step. The GPS data in three months period (April-June 2017) from the 22 permanent stations were used for this investigation. The contribution of selected stations is shown in Figure 1.

The real-time ZTDs estimated from those stations were compared with those PPP post-processing from PANDA software from Wuhan University (Jing-nan and Mao-rong, 2002).

In order to accurately transform ZTD into PWV, the meteorological data from meteorological stations and the local mean tropospheric temperature model (Tm) were evaluated for this study. The processing results were investigated to assess the quality of ZTD values derived from real-time PPP and to evaluate the data reliability from selected CORS stations.

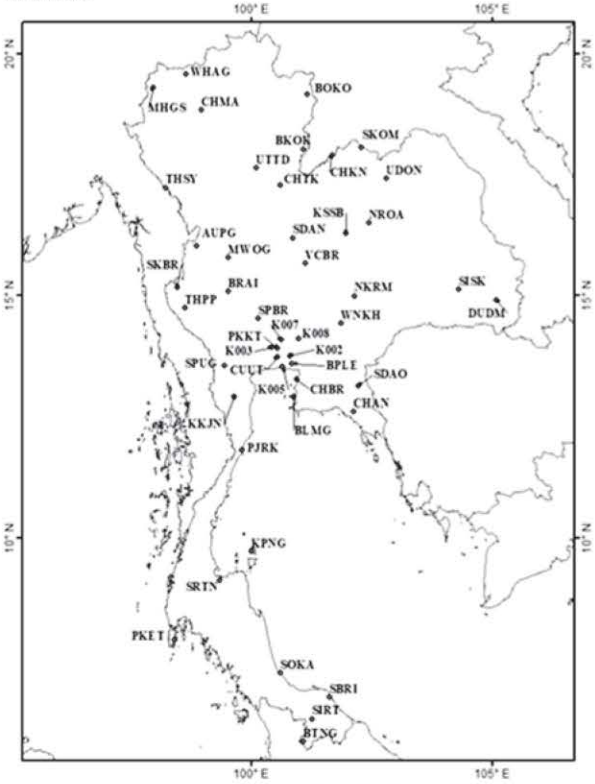

Figure 1: Location of selected GNSS CORS stations for this study (black dots)

2. Observation Model and Processing Strategy

2.1 Observation Equations

The GPS observation equations for PPP of the single dual-frequency receiver based on carrier phase (Φ) and pseudorange (P), respectively, can be expressed as the ionosphere-free code combinations and the ionosphere-free phase combinations to eliminate the first order ionospheric effects. For cm or mm precise level, some error sources have to be canceled or mitigated, such as antenna phase offsets and variations of satellites and receivers, phase wind-up, solid Earth tides, ocean loading, polar tides, Earth rotation parameter (ERP), and relativistic effects. If those error sources can be eliminated or accurately calculated with the empirical model, the simplified observation equations for PPP (Kouba, 2009) are shown in Equation (1)-(2).

$$\ell_P = \rho + c.(dt - dT) + T_r + \varepsilon_P$$

Equation 1

$$\ell_\Phi = \rho + c.(dt - dT) + T_r + N.\lambda + \varepsilon_\Phi$$

Equation 2

where ℓ_P and ℓ_Φ are the ionosphere-free combinations of pseudoranges and carrier phases, ρ is the geometrical range computed as a function of the satellite and receiver coordinates, c is the vacuum speed of light, dt and dT are the station receiver and satellite clock offsets from GPS time, T_r is the tropospheric path delay (ZPD), N is the non-integer ambiguity of the carrier-phase ionosphere-free combination, λ is the carrier-phase L3-combined wavelengths, ε_P and ε_Φ are the relevant measurement noise components, include multipath.

The ZPD can donate as a function of ZTD with mapping function (M), relating the tropospheric delay to the elevation angle of the satellite while replacing the known satellite clocks (dT) and coordinates according to the following mathematical model in the simplest form using Equation (3)-(4) (Kouba, 2009).

$$\ell_P = \rho + c.dt + M.ZTD + \varepsilon_P$$

Equation 3

$$\ell_\Phi = \rho + c.dt + M.ZTD + N.\lambda + \varepsilon_\Phi$$

Equation 4

In this study, The Ionosphere-free linear combinations together with Extended Kalman Filter (EKF) techniques in BNC software are used to estimate the receiver coordinate, the receiver clock bias, the non-integer ambiguity, and ZTD as unknown parameters where are solved for each observation epoch.

2.2 Tropospheric Delay Model

The troposphere is the lowest layer of the atmosphere. It has a distance above the Earth's surface of 8 km at the poles to 16 km height over the equator and consists of a dry and a wet component. About 90% of the tropospheric delay is caused by the dry or hydrostatic part, which is mainly a function of pressure (Hofmann-Wellenhof et al., 2008). The wet part depends on the water vapor, which is highly variable to the weather, climate and greenhouse effect, is difficult to model because of its high variability. The troposphere can cause path delays when radio signals propagate from GNSS satellites to the Earth's surface, regularly reaching a value of 2.3 m at the zenith and over 20 m at the low elevation angles (Yao et al., 2015). These effects depend on the real-valued refractive index (N) along with a signal ray path. The ZPD can be expressed as Equation (5).

$$ZPD = 10^{-6} \left(\int N_{dry} ds + \int N_{wet} ds\right)$$

Equation 5

where N_{dry} is the dry refractive index, N_{wet} is the wet refractive index, the integration is taken along the signal ray path. In GPS data processing, it is known that the ZPD is obtained from a zenith delay using proper mapping functions, which depend on the zenith angle of the satellite. There are the different atmospheric model using in mapping function, such as NMF (Niell Mapping Functions), VMF1 (Vienna Mapping Functions 1) or Ifadis (Mendes, 1998). Nonetheless, in the BNC software, the tropospheric mapping function is simplified as Equation (6) (Weber et al., 2016).

$$M = f(z) = 1/\cos(z)$$

Equation 6

where z is the zenith angle of the satellite. Consequently, the ZPD can be expressed as Equation (7). A priori ZTD can be obtained from the standard empirical models such as Hopfiled (1971), Niell (1996) and Saastamoinen (1972b) . The latter one has been applied in BNC software as Equation (7).

$$ZPD = 0.002277 \sec(z) \left[P + \left(\frac{1255}{T_s} + 0.05\right) e - B\tan^2 z\right] + \delta R$$

Equation 7

where P is the air pressure)unit: mbar), T_s is the temperature (unit: K), e is the partial pressure of water vapor (unit: mbar), B and δR are the correction terms that depend on z and the height of the station, respectively (Xu, 2007).

2.3 Converting the ZTD to the PWV

The ZTD derived from PPP can be expressed in two components as a Zenith Hydrostatic Delay (ZHD) and a Zenith Wet Delay (ZWD). The ZHD can be derived with a good accuracy with surface meteorological data. However, the ZWD is commonly used as an estimated parameter for higher accuracy due to a high variation and can be transformed into PWV with mean temperature (T_m).

The ZWD can be expressed in terms of the ZTD and ZHD (Bevis et al., 1992).

$$ZWD = ZTD - ZHD$$

Equation 8

Over the past two decades, there are several empirical ZHD models developed offering users the great flexibility of choice in their application (Chen and Liu, 2016). In this study, ZHD with the surface air pressure at the closet meteorological station is obtained from (Saastamoinen, 1972a) model as:

$$ZHD = \frac{2.27793P}{(1-0.00266cos(2\phi)-0.00028H)}$$

Equation 9

where ø is the latitude of the station (unit: radian), H is the height of the station above sea level (unit: m). The quantity of PWV above a receiver is usually stated as the vertically integrated mass of water vapor per unit area (e.g., in kilograms per square meter) or as the height of an equivalent column of liquid water. This quantity is related to the ZWD in the unit of length at the receiver (Bevis et al., 1994).

$$PWV = \prod * ZWD$$

Equation 10

where $\prod$ is the dimensionless constant of proportionality.

$$\prod = 10^6 M_w / (\rho_w R_v (k_2 - k_1 \frac{M_w}{M_d} + \frac{k_3}{T_m})$$

Equation 11

where ρ_w is the density of liquid water with values 10^3 kg.m^{-3}. R_v is the special gas constant of water vapor with values 461.51 JK^{-1}kg^{-1}. M_w and M_d are the molar mass of dry air and water vapor with values 0.00289644 kg.mol^{-1} and 0.018016 kg.mol^{-1}, respectively. k_1, k_2, and k_3 are the physical constant derived by several laboratories. In this study, the values 77.6900 K.hPa^{-1}, 71.2952 K.hPa^{-1}, 375463 K^2.hPa^{-1} for k_1, k_2, and k_3 are used . T_m is the weighted mean temperature of the atmosphere (unit: K).

$$T_m = \frac{\int \frac{e}{T} dz}{\int \frac{e}{T^2} dz}$$

Equation 12

To calculate the T_m from Equation (12), both e and T are extended from the surface to the top of the atmosphere which is not possible in the real-time retrieval of PWV values. An alternative way is used empirical model presented by (Bevis et al., 1994), Mendes et al., (2000) and GPT2w. Moreover, Yao et al., (2015) developed the GTm-III model to estimate T_m every location in the world. These models have been applied to several studies (Lu et al., 2015 and Yuan et al., 2014). Nevertheless, Tm determined from the empirical models is not as accurate as that directly obtained from the NWP models (Yuan et al., 2014).

In Thailand, Suwantong et al., (2016) derived the local T_m using AIRS and AMSU for GNSS-PWV estimation. The results show that the GNSS-PWVs derived from the local T_m model have the same level of the Root Mean Square Error (RMSE), which are comparable to the global T_m. Using the local T_m can reduce the mean bias from 1.06 mm to 0.20 mm. Thus, this model is applied in this study. The local T_m model is derived for the daytime as:

$$T_m = 0.6066 * T_s + 113.2914$$

Equation 13

and for the nighttime as:

$$T_m = 0.7938 * T_s + 57.4856$$

Equation 14

The surface temperature T_s can be obtained from an empirical model or meteorological sensor. The latter one was used in this study.

2.4 Software and Processing Step

In the preliminary study, The BKG NTRIP Client (BNC), developed by BKG (Weber et al., 2016), is capable of performing PPP in the real-time tool with some post-processing functionality, also retrieving real-time GNSS data streams from an IP address, a serial port or the NTRIP transport protocol. When using the PPP processing, some effects are not corrected by BNC, such as satellite antenna phase center variations, ocean and atmospheric loading, and polar tide. These error sources can affect the accuracy of the GNSS-derived ZTD estimates (Lu et al., 2015).

For this study, in order to obtain approximate reference coordinates of the CORS stations, 1-day batches of data were processed from the PANDA software. By using a 24-hour data set, the station coordinate accuracy within a centimeter level are used as a priori coordinate in subsequent processing. The BNC software in Figure 2 was used to process real-time PPP using data streams from 47 CORS stations of code and phase observations, the

broadcast ephemeris and CLK91 correction streams for satellite orbits and clocks. During the processing in BNC, these corrections from the real-time streams are applied to the broadcast ephemeris. Along with the precise position estimates, the estimated ZTD can also be obtained as one of the outputs. The ZTD values at the common epoch are compared to the PANDA-ZTD products at every 2 hours. The PWV values can be estimated by Equation (8)-(14) with local mean temperature and meteorological data (Table 1).

3.1 Real-Time PPP-ZTD Validation

In order to assess the quality of ZTD values derived from PPP technique with the real-time correction, we processed 47 CORS stations for the period of three months between April to June in 2017. The ZTD values were validated using the ZTD values from PANDA Software including outlier rejection procedures. The real-time ZTD solution derived from GNSS is 1 second while the PANDA-ZTD is sampled every 2 hours. Consequently, only the ZTD values at the same epoch were compared. The comparisons of the ZTD values derived from the PPP float solution and the PANDA-ZTD are shown in Table 2 and Figure 3. The results showed that mean bias and RMSE of the different ZTD values vary from -10.0 to 13.7 mm and 11.1 to 21.4 mm. Accordingly, for all 47 stations, the estimated ZTD values were accurate enough for the operational NWP model.

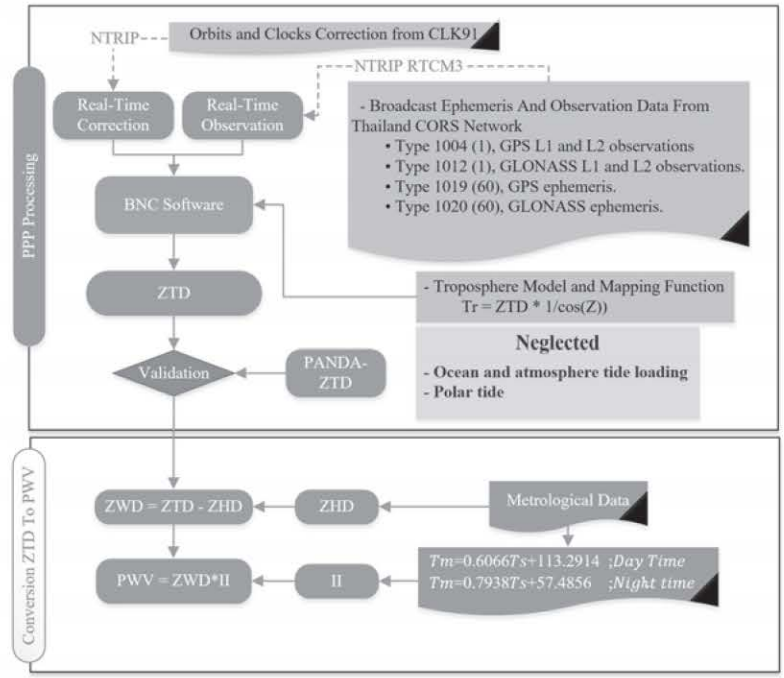

Figure 2: Data Processing Step to estimate the real-time ZTD/PWV values

Table 1: Configuration of the BNC software is used in this study

Configuration	Detail
Update cycle	Real-time
Output interval	1 s
GNSS used	GPS
Strategy	PPP
A Priori ZPD model	Saastamoinen
Troposphere mapping Function	1/cos(z)
Receiver PCV, PCO correction	Yes
Satellite PCV, PCO correction	Yes
Solid earth tide	Yes
Ocean tide loading and Polar tide	No
Input data format	RTCM-3
Input Orbit/Clock correction format	RTCM-SSR
Input broadcast ephemeris format	RTCM-SSR
Ambiguity resolution	No

Table 2: Mean Bias (mm), RMSE (mm) and Percentage of Value below 20 mm (The Threshold of Weather Nowcasting) of the Different ZTD Values between Real-Time PPP and PANDA. The underlined stations are shown the percentage of the different ZTD values greater than 85%.

Station	Bias	RMSE	% < 20mm
AUPG	2.1	18.5	79
BKOK	3.1	14.5	86
BLMG	6.7	15.6	80
BOKO	4	16.1	81
BPLE	-3.7	12.1	89
BRAI	8.5	16.7	81
BTNG	-7.3	13.6	83
CHAN	13.2	12.8	76
CHBR	-9.6	18.2	71
CHKN	0.8	14.4	87
CHMA	-5.7	17.4	78
CHTK	3.6	17.5	79
CUUT	-3.1	16.5	81
DUDM	4.9	15	82
K002	-1.9	15.6	80
K003	-1.1	15.3	85
K005	-2.5	13.3	87
K007	-3.9	16.7	81
K008	-2.2	14.7	85
KKJN	2.6	16.2	82
KPNG	-1.4	15.8	81
KSSB	3.9	17.8	79
MHGS	-8.2	14	79
MWOG	2.7	13.1	89
NKRM	-5	19.1	78
NROA	2.4	17.1	82
PJRK	13.3	12.5	71
PKET	9.2	15.5	80
PKKT	-3.7	12.7	90
PNRA	-5	11.1	91
SDAN	4	17.6	78
SDAO	2.8	18.7	77
SIRT	-5.7	13.6	83
SISK	-10	15.9	73
SKBR	4.2	20.4	77
SKOM	4.4	17	78
SOKA	-8.4	12.6	82
SPBR	13.7	14.5	68
SPUG	10.6	19.2	69
SRTN	-9.8	15.8	73
THPP	2.8	18.1	81
THSY	-2.4	17.2	80
UDON	-6.8	16	78
UTTD	-7.4	18.5	70
VCBR	5.4	14.8	83
WHAG	-4.2	13.4	87
WNKH	3.2	13.7	87

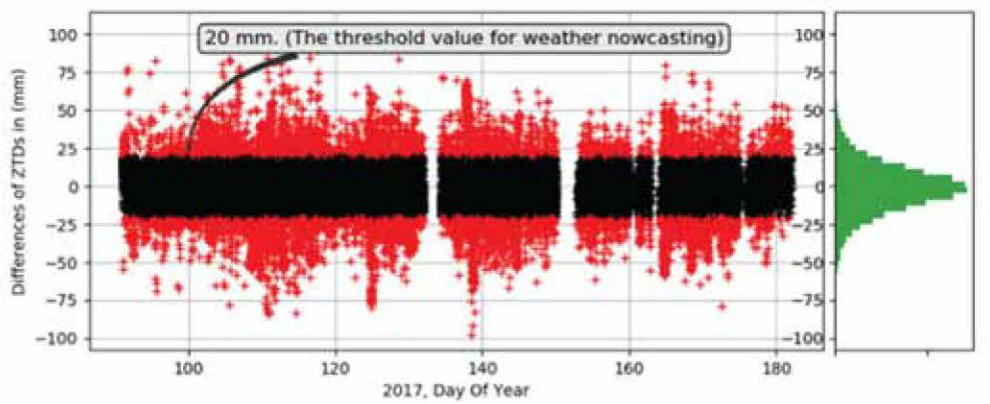

Figure 3: The differences of ZTDs of 47 CORS stations, about 80% of the real-time epoch solution, were within 20 mm (+ black dot) which is the threshold accuracy for PWV in weather nowcasting

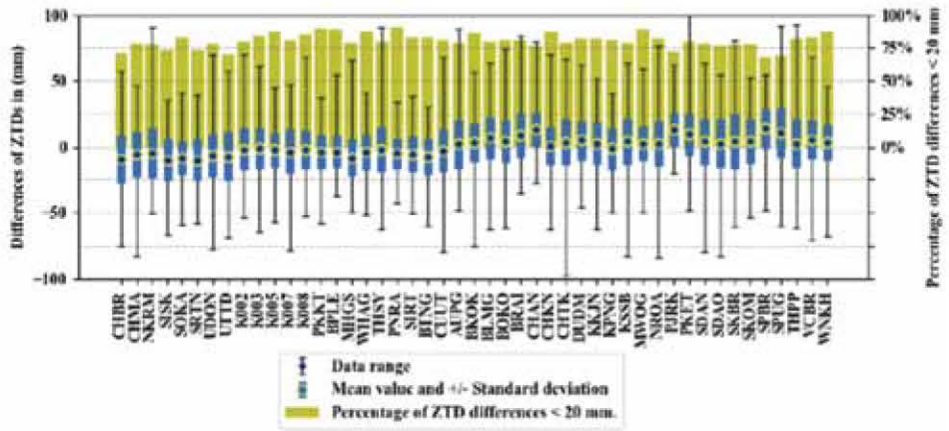

Figure 4: The statistic result and the percentage of differences of ZTD values of 47 CORS stations, during April-June in 2017.

According to (Yuan et al., 2014) 20 mm error in ZTD will result in an error of approximately 3 mm in PWV, which is the threshold accuracy for PWV in weather nowcasting (De Haan, 2006). We found that the average percentage of the different ZTD values within 20 mm is about 80% of the real-time epoch solution. We also found that nine stations (BKOK, BPLE, CHKN, K005, MWOG, PKKT, PNRA, WHAG, and WNKH), above 85% of the real-time epoch solution, are found within the 20 mm. Consequently, we concluded that about 20% of the real-time epoch solutions could not be applied in the meteorological applications. To improve the accuracy of the real-time ZTD, the real-time GNSS data processing strategy need to be carefully developed (Figure 4).

The accuracy of ZTD values in our data processing is depended on the real-time corrected observations and corrections. If the data processing center is lost the internet connection to CORS station or the correction service, this will degrade the accuracy of the real-time epoch solution and cause the large variation in data processing. Especially, the CORS stations in the remote area can be insufficient internet stability. In addition, the quality of observation data streaming from CORS stations also affects the accuracy of the output solution such as data gap, satellite geometry, and satellite availability.

3.2 Estimation of Precipitable Water Vapor

The PWV values derived from the real-time PPP technique using local mean temperature by Equation (13)-(14) and meteorological data are shown in Figure 5. The results showed that the PWV values from the most stations varied from 10 to 80 mm. Figure 6 illustrates the PWV values from 47 stations during a period of three months. The PWV values increased from about 50 to 70 mm between DOY 96 to DOY 130 because of changing season from the hot season to the rainy season and the influence of the southwest monsoon brings heavy storms.

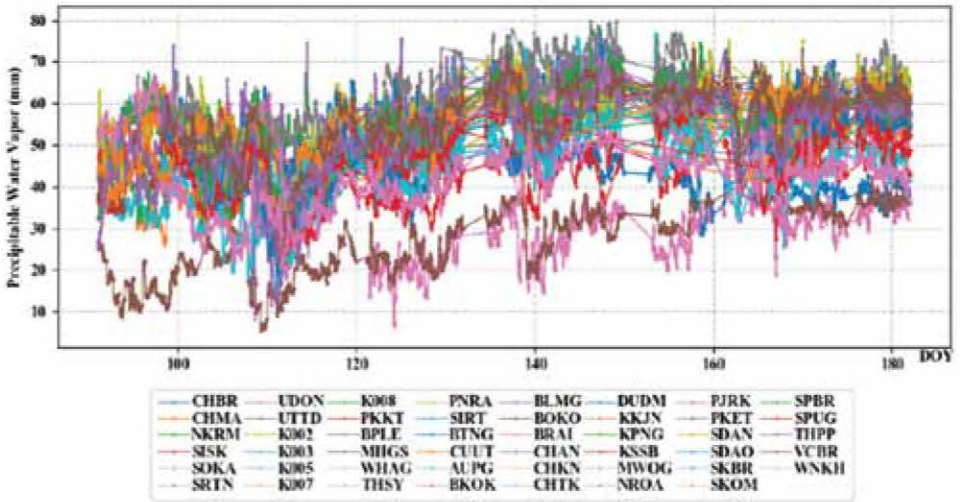

Figure 5: PPP-PWV derived from GPS using local mean temperature and local meteorological data, during April-June in 2017

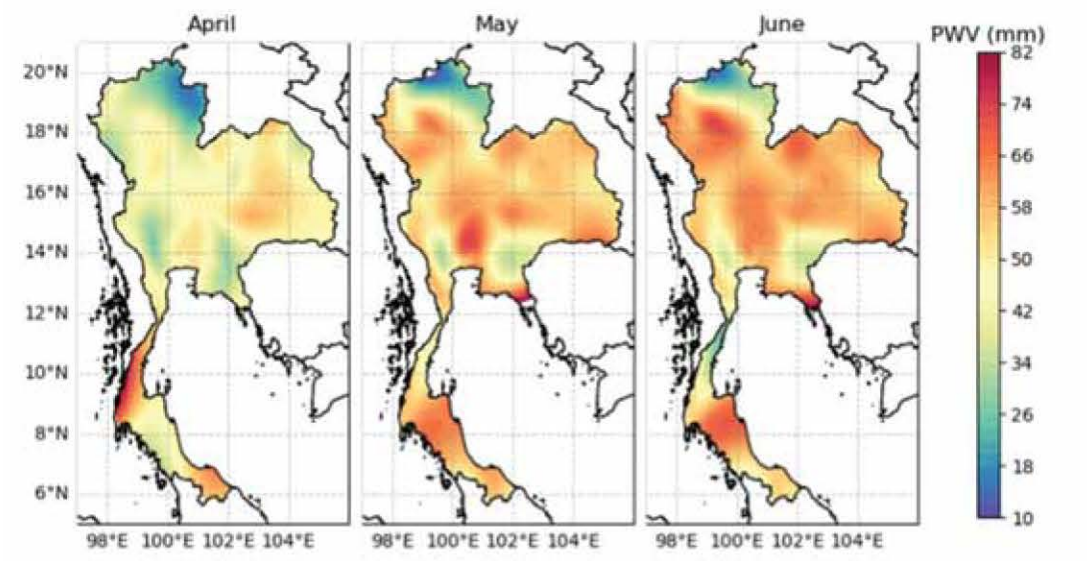

Figure 6: The amount of the PWV values between April to June in 2017, where a southwest monsoon period occurred over Thailand

Thailand had been conducted. The three months of GPS observation data from selected 47 CORS stations were used in data processing together with the CLK91 real-time correction. The ZTD values can be estimated along with unknown parameter using PPP technique within BNC software. The ZTD values had been compared by the PANDA-ZTD software as the reference values at 2-hour interval. The results showed that the average of RMSE and Mean Bias were about 15.6 mm and 0.28 mm, respectively. Thus, the quality of ZTD satisfied with the threshold requirements (20 mm) for the NWP model (De Haan, 2006). However, the different ZTD values, about 20% of the real-time epoch solutions, were not accurate enough for applying in the operational NWP model.

The estimated PWV over three months showed the seasonal and temporal variation in the water vapor content in the atmosphere. In order to get the high accuracy of the real-time ZTD/PWV using GNSS observation data, it still remains a challenging task at a space and time resolution, due to high variation of PWV in this mid-latitude. In this research, the data processing strategy needs to be implemented to increase the accuracy of output solutions. Further research of a long-term ZTD/PWV series will be focused on improving the real-time ZTD/PWV products, more accurate and stable for support meteorological applications.

Acknowledgments

We acknowledge the Department of Land (DOL) and the Department of Public Works and Town& Country Planning (DPT) for providing the GNSS data and the IGS for providing real-time orbit and clock products. This paper is based on the paper presented at the 33rd ITC-CSCC 2018, July 4-7, Bangkok, Thailand.

References

Bennitt, G. V. and Jupp, A., 2012, Operational Assimilation of GPS Zenith Total Delay Observations into the Met Office Numerical Weather Prediction Models. *Monthly Weather Review*, Vol. 140(8), 2706-2719. doi:10.1175/mwr-d-11-00156.1

Bevis, M., Businger, S., Herring, T. A., Rocken, C., Anthes, R. A. and Ware, R. H., 1992, GPS Meteorology: Remote Sensing of Atmospheric Water Vapor Using the Global Positioning System. *Journal of Geophysical Research-Atmospheres*, Vol. 97, 15. doi:10.1029/92JD01517

Bevis, M., Businger, S., Chiswell, S., Herring, T. A., Anthes, R. A., Rocken, C. and Ware, R. H., 1994, GPS Meteorology: Mapping Zenith Wet Delays onto Precipitable Water. *Journal of Applied Meteorology*, Vol. 33(3), 379-386. doi:10.1175/1520-0450(1994)033<0379:gmmzwd>2.0.co;2

Chen, B. and Liu, Z., 2016, A Comprehensive Evaluation and Analysis of the Performance of Multiple Tropospheric Models in China Region. *Ieee Transactions on Geoscience and Remote Sensing*, Vol. 54(2), 663-678. doi:10.1109/Tgrs.2015.2456099

De Haan, S., 2006, National/Regional Operational Procedures of GPS Water Vapour Networks And Agreed International Procedures. WMO/TD No. 1340, KNMI, Netherlands, 20.

Dousa, J. and Vaclavovic, P., 2014, Real-time Zenith Tropospheric Delays in Support of Numerical Weather Prediction Applications. *Advances in Space Research*, Vol. 53(9), 1347-1358. doi: http://dx.doi.org/10.1016/j.asr.2014.02.021

Elgered, G., Davis, J. L., Herring, T. A. and Shapiro, I. I., 1991, Geodesy by Radio Interferometry: Water Vapor Radiometry for Estimation of The Wet Delay. *Journal of Geophysical Research: Solid Earth*, Vol. 96(B4), 6541-6555. doi:10.1029/90jb00834

Gendt, G., Dick, G., Reigber, C., Tomassini, M., Liu, Y. and Ramatschi, M., 2004, Near Real Time GPS Water Vapor Monitoring for Numerical Weather Prediction in Germany. *Journal of the Meteorological Society of Japan*. Ser. II, Vol. 82(1B), 361-370. doi:10.2151/jmsj.2004.361

Grinter, T. and Roberts, C., 2013, Real Time Precise Point Positioning: Are We There Yet. Paper presented at *the International Global Navigation Satellite Systems Society IGNSS Symposium 2013*, Outrigger Gold Coast, Qld, Australia, 16 – 18 July 2013.

Hagemann, S., Bengtsson, L. and Gendt, G., 2002, On the Determination of Atmospheric Water Vapour from GPS measurements. Journal of Geophysical Research Atmospheres, Vol. 108(21). DOI: 10.1029/2002JD003235

Hofmann-Wellenhof, B., Lichtenegger, H. and Wasle, E., 2008, *Global Navigation Satellite Systems GPS, GLONASS*, Galileo and more. Austria: Springer-Verlag Wien.

Hopfield, H. S., 1971,. Tropospheric Effect on Electromagnetically Measured Range: Prediction from Surface Weather Data. *Radio Science*, Vol. 6(3), 357-367. doi:10.1029 /RS006i003p00357

Jing-nan, L. and Mao-rong, G., 2002, PANDA Software and Its Preliminary Result of Positioning and Orbit Determination. *Wuhun University Journal of Natural Sciences*, Vol. 8, 603-609.

Kitpracha, C., Promchot, D., Srestasathiern, P. and Satirapod, C., 2017, Precise Tropospheric Delay Map of Thailand Using GNSS Precise Point Positioning Technique. *International Journal of Geoinformatics*, Vol. 13(2), 17-21.

Kouba, J., 2009, A Guide To Using International GNSS Service (IGS) products.

Li, W., Yuan, Y., Ou, J., Li, H. and Li, Z., 2012, A New Global Zenith Tropospheric Delay Model IGGtrop for GNSS Applications. *Chinese Science Bulletin*, Vol. 57(17), 2132-2139. doi:10.1007/s11434-012-5010-9

Li, X., Dick, G., Lu, C., Ge, M., Nilsson, T., Ning, T., Wickert, J. and Schuh, H., 2015, Multi-GNSS Meteorology: Real-Time Retrieving of Atmospheric Water Vapor From BeiDou, Galileo, GLONASS, and GPS Observations. *Ieee Transactions on Geoscience and Remote Sensing*, Vol. 53(12), 6385-6393. doi:10.1109/Tgrs.2015.2438395

Lu, C. X., Li, X., Nilsson, T., Ning, T., Heinkelmann, R., Ge, M. R., Glaser, S. and Schuh, H., 2015, Real-Time Retrieval of Precipitable Water Vapor from GPS and BeiDou Observations. *Journal of Geodesy*, Vol. 89(9), 843-856. doi:10.1007/s00190-015-0818-0

Mendes, V. B., 1998, *Modeling the Neutral-Atmosphere Propagation Delay in Radiometric Space Techniques*. (Ph.D. dissertation), Department of Geodesy and Geomatics Engineering Technical Report No. 199, University of New Brunswick, Fredericton, New Brunswick, Canada.

Mendes, V. B., Prates, G., Santos, L. and Langley, R. B., 2000, An Evaluation of the Accuracy of Models for the Determination of Weighted Mean Temperature of the Atmosphere. *Proceedings of ION 2000 National Technical Meeting.*

Meunram, P., and Satirapod, C., 2018, Variation of Precipitable Water Vapor derived from GNSS CORS Observations in Thailand. *Paper presented at the ISGNSS2018*, Bali, Indonesia.

Niell, A. E., 1996, Global Mapping Functions for the Atmosphere Delay at Radio Wavelengths. *Journal of Geophysical Research: Solid Earth*, Vol. 101(B2), 3227-3246. doi:10.1029/95 JB03048

Rohm, W., Yuan, Y., Biadeglgne, B., Zhang, K. and Marshall, J. L., 2014, Ground-based GNSS ZTD/IWV Estimation System for Numerical Weather Prediction in Challenging Weather Conditions. *Atmospheric Research*, Vol. 138, 414-426. doi:10.1016/j.atmosres.2013.11.026

Saastamoinen, J., 1972a, Atmospheric Correction for the Troposphere and Stratosphere in Radio Ranging Satellites. Vol. 15, 247-251. doi:10.1029 /GM015p0247

Saastamoinen, J., 1972b, Contributions to the Theory of Atmospheric Refraction. Bulletin Géodésique (1946-1975), Vol. 105(1), 279-298. doi:10.1007/bf02521844

Satirapod, C., Anonglekha, S., Choi, Y.-S. and Lee, H.-K., 2011, Performance Assessment of GPS-Sensed Precipitable Water Vapor using IGS Ultra-Rapid Orbits: A Preliminary Study in Thailand. *Engineering Journal*, Vol. 15(1), 1-8. doi:10.4186/ej.2011.15.1.1

Shi, J., Xu, C., Guo, J. and Gao, Y., 2015, Real-Time GPS Precise Point Positioning-Based Precipitable Water Vapor Estimation for Rainfall Monitoring and Forecasting. *Ieee Transactions on Geoscience and Remote Sensing*, Vol. 53(6), 3452-3459. doi:10.1109/ TGRS.2014.2377041

Suwantong, R., Satirapod, C., Srestasathiern, P. and Kitpracha, C., 2016, Deriving the Mean Tropospheric Temperature Model using AIRS and AMSU for GNSS Precipitable Water Vapour Estimation. ION GNSS+ 2016, Sept. 12-16, Portland, Oregon.

Weber, G., Mervart, L., Stürze, A., Rülke, A. and Stöcker, D., 2016, BKG Ntrip Client, Version 2.12. Mitteilungen des Bundesamtes für Kartographie und Geodäsie. Vol. 49, Frankfurt am Main, 2016.

Xu, G., 2007, GPS Theroy Algorithms and Applications (2nd ed.). Germany: Krips bv, Meppel.

Yao, Y., Zhang, B., Xu, C., He, C., Yu, C. and Yan, F., 2015, A Global Empirical Model for Estimating Zenith Tropospheric Delay. *Science China Earth Sciences*, Vol. 59(1), 118-128. doi:10.1007/s11430-015-5173-8

Yuan, Y. B., Zhang, K. F., Rohm, W., Choy, S., Norman, R. and Wang, C. S., 2014, Real-Time Retrieval of Precipitable Water Vapor from GPS Precise Point Positioning. *Journal of Geophysical Research-Atmospheres*, Vol. 119(16), 10044-10057. doi:10.1002/2014JD 021486

Zumberge, J. F., Heflin, M. B., Jefferson, D. C., Watkins, M. M. and Webb, F. H., 1997, Precise Point Positioning for the Efficient and Robust Analysis of GPS Data from Large Networks. *Journal of Geophysical Research: Solid Earth*, Vol. 102(B3), 5005-5017. doi:10.10 29/96JB03860